

Nanoscale Characterization of Ferroelectric Domain Structures Using Scanning Near-field Optical Microscopy

Minoru Osada*, Yuji Noguchi**, Shingo Katayama** and Masaru Miyayama**

Advanced Materials Laboratory, National Institute for Materials Science, Tsukuba, Ibaraki 305-0044, Japan
Fax: 81-29-854-9061, e-mail: osada.minoru@nims.go.jp

*PRESTO, Japan Science and Technology Agency, Kawaguchi, Saitama 332-0012, Japan

**Research Center for Advanced Science and Technology, University of Tokyo, Tokyo 153-8904, Japan

We present a new approach to nanoscale domain characterization using Raman scattering with scanning near-field optical microscopy (SNOM). In $\text{Bi}_4\text{Ti}_3\text{O}_{12}$ (BIT) single crystals, we find that the polarization dependence of Raman spectra exhibits local symmetries that reflect domain structures. Moreover, Raman spectra at domain walls exhibit local symmetry breaking due to the presence of oxygen vacancies, and planer defects, due to oxygen vacancies, that accumulated near domain walls cause a strong domain pinning. These SNOM-Raman results shed new light on understanding of domain structures in BIT.

Keywords: SNOM, Raman scattering, $\text{Bi}_4\text{Ti}_3\text{O}_{12}$ (BIT), nanoscale domain structures

1. INTRODUCTION

Nanoscale characterization is one of current topics in the ferroelectric field. In particular, recent progress in oxide electronic devices such as MEMS, FeRAM requires detailed understanding of local ferroelectric properties on the nanoscale level. This has motivated a number of studies on nanostructures (like nanodots, nanoislands, nanowires, etc.) with various scanning probe microscopy (SPM) techniques [1].

The most widely used technique is piezoresponse force microscopy (PFM), which is a very effective tool for local characterization of both polarization and piezoelectric properties [2]. Recently, other SPM techniques with surface capacitance and non-linear dielectric measurements have been applied for nanoscale characterization of polarization components [3,4]. On the other hand, scanning near-field optical microscopy (SNOM) [5] is rather new technique in the ferroelectric field, and the applications are still limited cases [6,7]. In the case of micro-scale studies, however, optical techniques such as polarized microscopy, light scattering and SHG were well established, and provided various important information on ferroelectric properties. Therefore, the combination of SNOM with these optical techniques is very promising even for nano-researches. Here, we focus on combining SNOM technique with Raman scattering, and provide a new approach of SNOM Raman scattering for nanoscale domain imaging.

Raman spectroscopy is extremely useful for studies of ferroelectric properties [8,9]. Usually, Raman modes are local in character, and each structural unit participates in each mode. Thus, Raman spectroscopy is often used to study local structural changes such as phase transition, doping, disordering, defect. Also, Raman spectroscopy is

the most suitable technique for the observation of soft mode, which is closely linked to polarization properties. With these characters of Raman spectroscopy, one can obtain fundamental structural parameters related to ferroelectric properties. We also note that Raman spectroscopy is a powerful technique for characterization of domain structures [10,11]. This is based on Raman-selection rule. In general, Raman scattering intensity is expressed by tensor component of ion polarizability. Thus, the intensity of Raman mode basically reflects polarized vector of domains. In such a way, we can easily distinguish domain structures.

In this study, we applied SNOM-Raman technique to nanoscale domain characterization in $\text{Bi}_4\text{Ti}_3\text{O}_{12}$ (BIT) single crystals. Our focus is placed on characterization of domain walls. It has been recognized that ferroelectric domain walls are very thin, typically one or a few lattice constant [1]. This length scale is actually beyond the sub-wavelength resolution of SNOM. However, since wall-induced elastic strains or internal fields are much widely distributed, these changes can be detected even with optical signal. In particular, SNOM Raman scattering is ideally suited for studying domain walls, as it provides information on local structure and local symmetry of domain walls. In addition, SNOM-Raman data might shed some light on microscopic information on defects in terms of their geometric structure and their influence on domain dynamics. In BIT case, oxygen vacancies almost always have negative impacts on ferroelectric properties such as domain pinning and fatigue problem [12,13]. Even though the importance of oxygen vacancies on ferroelectric properties is generally accepted, a microscopic experimental characterization of these defects is still lacking. We will also address this defect issue.

2. EXPERIMENTAL

2.1. SNOM Raman scattering

SNOM used in this study is a new technique for nanoscale optical characterization [5]. The basic technique involves local excitation of evanescent light using a fiber nano-probe. Excited light is surface-localized and confined in nanoscale, thus providing unique opportunity for nanoscale spectroscopy.

The experimental setup for SNOM-Raman measurement is shown in Fig. 1. Our SNOM system, based on a commercial SNOM (Omicron, Twin-SNOM), is specially upgraded for spectroscopy purpose. The gold-coated fiber probe, forming the SNOM aperture, can be moved with nanometer accuracy to and from the surface. Single-mode fiber probes capable of linear polarized light output ($\sim 20\%$) were selected for use in the experiment. The SNOM probe is held within 10 nm of the sample surface using the shear-force feedback technique. The 514.5-nm line from an Ar⁺ laser was used as an excitation source. Raman-scattered light was detected in a backscattering configuration using the reflective objective lens and then passed through a holographic notch filter (Kaiser, SuperNotch-Plus) to remove elastically scattered light before being focused into the spectrometer. A thermo-cooled intensified CCD camera (Andor Technology, DV438) was used in conjunction with a Czerny-Turner spectrometer for the Raman signal detection.

The key challenge presented by the SNOM Raman technique lies in the detection of the very low signal levels which are concomitant with the very low intensity of the sub- $\lambda/2$ light source and the low scattering cross section of the Raman effect. For the work presented in this paper, a probe with an estimated aperture of 50–70 nm was employed; this delivered of the order a few μW of 514.5-nm

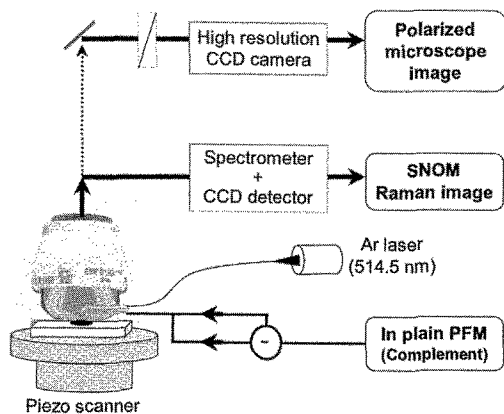


Fig. 1. The experimental setup for SNOM-Raman measurement.

radiation to the sample. Special care was also taken in the design of the collection optics. The use of the reflective objective lens is quite powerful since it offers high yield light detection with $> 80\%$ of usage near-field light [14]. Fig. 2 presents a test example, in which we use single-wall carbon nanotube (SWNT) to check the sensitivity of our system. In this case, we can detect Raman signal even from individual SWNT. From a comparison between Raman image and topography, Raman image clearly distinguishes dispersion of SWNT, and the spatial resolution of ~ 30 nm is comparable with topography. This kind of Raman imaging is interesting because it offers very detailed information on chemical structure and surface topography at the same time. We also note that SNOM has additional advantages for non-contact means with convenience for *in-situ* characterization. These features are quite important for characterization of practical devices.

2.2 Samples and characterization

The material studied here is $\text{Bi}_4\text{Ti}_3\text{O}_{12}$ (BIT), a promising material because of its high Curie temperature (T_C) and large spontaneous polarization (P_S) [15,16]. BIT single crystals grown by a self-flux method, were cut so as to align the major P_S direction with the a axis, where the crystallographic axis was determined with polarized optical microscopy. Prior to SNOM-Raman experiments, Raman selection rule of domain structures were characterized by a conventional micro-Raman system (Jobin-Yvon T64000). Complementary data were also obtained from PFM using SII, SPI3800, where the direction of P_S in the a - b plane was elucidated. Details of preparation and characterization are described elsewhere [17].

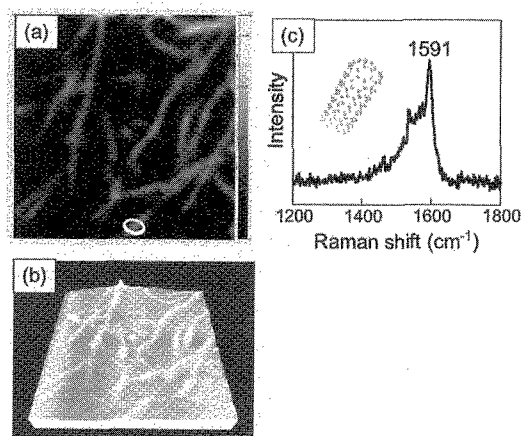


Fig. 2. Simultaneous topographic image (a) and SNOM Raman image (b) of SWNTs dispersed on Si substrate. Scan area is 600×600 nm. (c) Raman spectra taken from the individual SWNT [at the marked area in (a)]. The Raman image is acquired by detecting the intensity of G band (at 1591 cm^{-1}).

3. RESULTS AND DISCUSSION

3.1. Raman selection rule of domain structures in $\text{Bi}_4\text{Ti}_3\text{O}_{12}$

At the starting point of domain studies, we identify Raman selection rule of the domain structures. Fig. 3 compares polarized Raman spectra measured for the xx , yy and zz polarization configurations ($x //$ polar axis). The Raman spectra exhibit intense phonon modes (at 30, 60, 80-150, ~ 260 , ~ 520 and 840 cm^{-1}) and many weak features. Clearly, the external and internal modes, which stem from $[\text{Bi}_2\text{Ti}_3\text{O}_{10}]$ units and $(\text{Bi}_2\text{O}_2)^{2+}$ layers [18,19], show different response to polarization vector. In particular, the highest mode at 840 cm^{-1} , which is assigned to the c -axis symmetric stretching vibrations of the TiO_6 octahedra, appears exclusively for the zz polarization configuration. Also, the marked dependence of the TiO_6 -octahedra modes is observed in the ab -plane, which predominantly contributes to polarization property of BIT. The most prominent change concerns highly anisotropic nature of the soft phonon ($\sim 30 \text{ cm}^{-1}$) and TiO_6 mode ($\sim 520 \text{ cm}^{-1}$); these modes appear exclusively for the xx polarization configuration ($x //$ polar axis). Moreover, these modes consist of the displacement of the TiO_6 octahedra, which is closely linked to the P_S . Thus, these results clearly indicate that the Raman spectra can be used as a fingerprint of the symmetry of domain structures.

3.2. Nanoscale characterization of domain structures in $\text{Bi}_4\text{Ti}_3\text{O}_{12}$

We now turn to the applicability of SNOM Raman spectroscopy for nanoscale domain characterization in $\text{Bi}_4\text{Ti}_3\text{O}_{12}$. Fig. 4(a) shows the optical image of investigated crystal, which consists of striped 90° domains and needle-type domains. We choose typical points at the domain interior (A and B), and investigated polarization properties by SNOM Raman measurements. Fig. 4(b) compares Raman spectra taken from both A and B points.

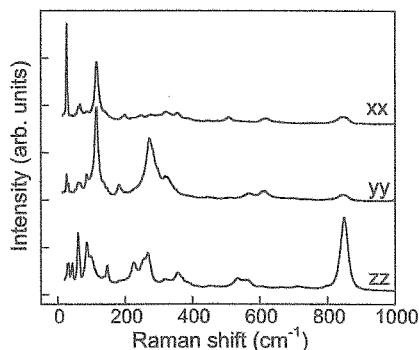


Fig. 3. Polarized Raman spectra measured for the xx , yy and zz polarization configurations. Spectra were acquired with conventional micro-Raman measurements.

From a comparison with polarization studies in Fig. 3, the polarization dependence of Raman spectra exhibits local symmetries that reflect domain structures. The spectrum of point A [Fig. 4(b)] gives rise to the observation of the in-plane TiO_6 mode. This polarized spectrum was quite reproducible, and was in agreement with xx configuration (Fig. 3), indicating the a -domain state of this region. At the point B, the spectrum [lower spectrum in Fig. 4(b)] resembles the one rather close to the yy configuration. These differences in the spectral features between A and B clearly indicate the rotation of the crystallographic axes associated with the 90° domain walls.

We also investigate the structure of domain walls. In Fig. 4(b) we compare Raman spectra taken from domain wall (point C) and domain interior (points A, B). Clearly, Raman spectra at domain walls exhibit local symmetry breaking. Of the most notable is the highest-frequency TiO_6 mode (at 840 cm^{-1}), which shows clear two-mode behavior with the appearance of new mode (marked by an arrow). From our preliminary PFM analysis, this region is related to 180° -domain wall with head-to-head or tail-to-tail configuration. Usually, this kind of “charged” domain wall strongly interacts with oxygen vacancies. Thus, the newly observed mode is associated with symmetry breaking, due to oxygen vacancies at the domain wall.

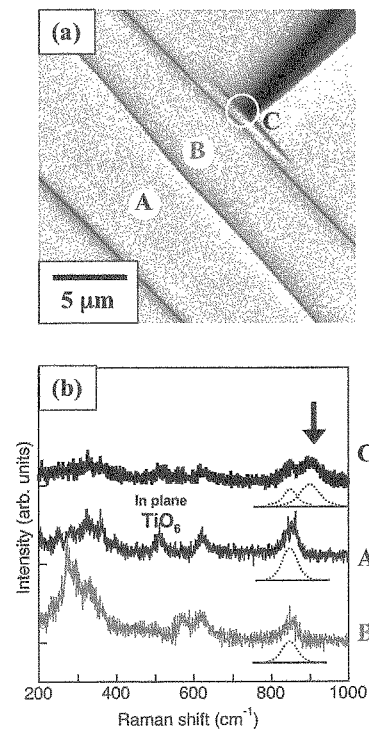


Fig. 4. (a) Optical image of investigated BIT crystal, which consists of striped 90° domains and needle-type domains. (b) SNOM-Raman spectra taken from domain interior (points A, B) and domain wall (point C).

We now consider the possible origin of the defect-induced mode. The 840-cm^{-1} TiO_6 mode is associated with the oxygen vibration of the TiO_6 octahedra. Also considering Raman selection rule in triple layers of perovskite units, the outside TiO_6 octahedra are normally Raman-active, but the inside one is forbidden. Thus, the main Raman band (at 840 cm^{-1}) comes from the outside octahedra. On the other hand, the defect-induced mode can be assigned to the vibration of the oxygen vacancy at the inside octahedra. Actually, this picture of the defect structure is in good accordance with recent structural studies [13]. From detailed structural study based on neutron diffraction and *ab-initio* calculation, the inside octahedra have much lower energy for vacancy formation, and the dominant defect species are oxygen vacancies at the inside octahedra [O(1) site]. These results demonstrate the usefulness of SNOM-Raman spectroscopy for the study of nanoscale domain structures, including detailed information on domain walls and defects.

3.3. Nanoscale domain imaging in $\text{Bi}_4\text{Ti}_3\text{O}_{12}$

We note that Raman imaging provides another perspective of detailed domain pictures near domain walls. Fig. 5(a) represents Raman-intensity mapping of the defect-induced mode ($\text{V}\delta$) near point C in Fig. 4(a). As discussed, this mode is intimately linked to oxygen vacancies, and Fig. 5(a) thus provides some information on vacancy distribution. Clearly, an abrupt change in the $\text{V}\delta$ -mode intensity occurs at the domain walls, and the highest intensity is located at needle-end. Thus, oxygen vacancies are highly accumulated near the needle-end, which is associated with domain pinning sites. We also note that the $\text{V}\delta$ mode is widely distributed along domain walls.

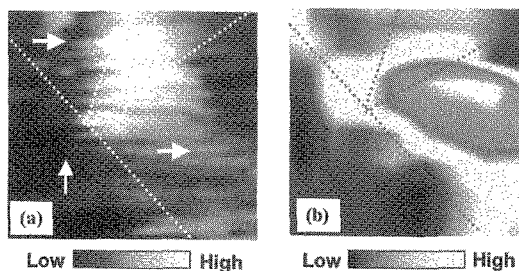


Fig. 5. SNOM Raman imaging for the intensity (a) and frequency (b) of the defect-induced mode ($\text{V}\delta$) near point C in Fig. 4(a). Scan area is 500×500 nm. The Raman images are acquired by detecting the intensity and frequency of the $\text{V}\delta$ mode (at 880 cm^{-1}). The $\text{V}\delta$ mode is intimately linked to oxygen vacancies, and these images provide information on $\text{V}\delta$ distribution and $\text{V}\delta$ -induced strain energy.

In Fig. 5(b) we also investigate the distribution in the $\text{V}\delta$ -mode frequency. Since Raman frequency is quite sensitive to stress or strain energy, Fig. 5(b) shed new light on pinning effects or strain effects. From a comparison between two images [Figs. 5(a) and 5(b)], there is some similarity. As with the $\text{V}\delta$ distribution, the strain field is highly localized along domain walls (or pinning sites). This is a clear signature for strain-field effects due to pinning of oxygen vacancies, and planer defects (due to oxygen vacancies) that accumulated near domain walls cause a strong domain pinning. We believe that these SNOM-Raman data are the first spectroscopic evidence for geometrical structure of domain walls and location of oxygen vacancy.

4. SUMMARY

We have utilized SNOM-Raman scattering to nanoscale domain characterization. In $\text{Bi}_4\text{Ti}_3\text{O}_{12}$ (BIT) single crystal, we find that the polarization dependence of Raman spectra exhibits local symmetries that reflect domain structures. Raman spectra at domain walls exhibit local symmetry breaking due to the presence of oxygen vacancies. Moreover, SNOM-Raman imaging demonstrate the usefulness of SNOM-Raman spectroscopy for the study of nanoscale domain structures, including vacancy distribution, strain field, pinning effects near domain walls. These SNOM-Raman results shed new light on understanding of domain structures in BIT.

REFERENCES

- [1] For a review, "Nanoscale characterization of ferroelectric materials", M. Alexe and A. Gruverman (Eds.) (Springer-Verlag, Berlin, 2004).
- [2] C. Harnagea and A. Pignolet, "Challenges in the analysis of the local piezoelectric response", Chap. 2 in Nanoscale characterization of ferroelectric materials, M. Alexe and A. Gruverman (Eds.) (Springer-Verlag, Berlin, 2004).
- [3] S. V. Kalinin and D. A. Bonnell, "Electric scanning probe imaging and modification of ferroelectric surface", Chap. 1 in Nanoscale characterization of ferroelectric materials, M. Alexe and A. Gruverman (Eds.) (Springer-Verlag, Berlin, 2004).
- [4] Y. Cho, "Scanning nonlinear dielectric microscopy for investigation of ferroelectric polarization", Chap. 5 in Nanoscale characterization of ferroelectric materials, M. Alexe and A. Gruverman (Eds.) (Springer-Verlag, Berlin, 2004).
- [5] E. Betzig, M. Isaacson and A. Lewis, Appl. Phys. Lett. **51**, 2088 (1987).
- [6] T. J. Yang, U. Mohideen and M. C. Gupta, Appl.

- Phys. Lett. **71**, 1960 (1997).
- [7] X. K. Orlik, M. Labardi and M. Allegrini, Appl. Phys. Lett. **77**, 2042 (2000).
- [8] P. S. Dobal and R. S. Katiyar, J. Raman Spectroscopy **33**, 405 (2002).
- [9] M. Osada, "Raman spectroscopy as a unique tool for characterization of ferroelectric materials", in *Advanced materials for optoelectronics*, R. Jayavel and K. Kitamura (Eds.) (Vilay Nicole, 2005).
- [10] M. Osada, M. Tada, M. Kakihana, Y. Noguchi and M. Miyayama, Mater. Eng. Sci. B **120**, 95 (2005).
- [11] M. Osada, K. Nishida, S. Wada, S. Okamoto, R. Ueno, H. Funakubo and T. Katoda, Appl. Phys. Lett. **87**, 232902 (2005).
- [12] B. H. Park, B. S. Kang, S. D. Bu, T. W. Noh, J. Lee and W. Jo: Nature (London) **401**, 682 (1999).
- [13] Y. Noguchi, T. Matsumoto and M. Miyayama, Jpn. J. Appl. Phys. **44**, L570 (2005).
- [14] More information is available at <http://www.omicron.de/index2.html>.
- [15] S. E. Cummins and L. E. Cross: J. Appl. Phys. **39** (1968) 2268.
- [16] H. Irie, M. Miyayama and T. Kudo: J. Appl. Phys. **90** (2001) 4089.
- [17] M. Soga, Y. Noguchi, M. Miyayama, H. Okino, and T. Yamamoto, Appl. Phys. Lett. **84**, 100 (2004).
- [18] S. Kojima, R. Imaizumi, S. Hamazaki and M. Takashige: Jpn. J. Appl. Phys. **33**, 5559 (1994).
- [19] M. Osada, M. Tada, M. Kakihana, T. Watanabe and H. Funakubo, Jpn. J. Appl. Phys. **40**, 5572 (2001).

(Received December 10, 2005; Accepted January 31, 2006)